Mon. Not. R. Astron. Soc. **356,** 1177–1190 (2005) doi:10.1111/j.1365-2966.2004.08549.x

Two-dimensional warm gas kinematics in interacting galaxy systems

R. Rampazzo,[1⋆] H. Plana,[2] P. Amram,[3] S. Bagarotto,[1] J. Boulesteix[3] and M. Rosado[4]

[1]*Osservatorio Astronomico di Padova, Vicolo dell'Osservatorio 5, I-35122 Padova, Italy*
[2]*Department Ciências Exatas e Tecnológicas, Universidade Estadual de Santa Cruz, Ilheus, BA, Brazil*
[3]*Observatoire Astronomique de Marseille–Provence and Laboratoire d'Astrophysique de Marseille, 2 Place Le Verrier, 13248 Marseille Cedex 04, France*
[4]*Instituto de Astronomia, UNAM, Apartado Postal 70-264, Ciudad Universitaria, México DF, CP 04510, Mexico*

Accepted 2004 October 24. Received 2004 October 19; in original form 2004 June 7

ABSTRACT

Gas reservoirs, internal or acquired, play an important role in the secular evolution of interacting galaxies, since they are able to enhance/trigger star formation episodes and, probably, feed the activity of active galactic nuclei. Using Fabry–Perot observations, we have mapped, in the Hα line, the warm ($T \approx 10^4$) gas distribution and the velocity fields of the galaxy members of five interacting, gas-rich galaxy systems. We investigated two M51-like systems (Arp 70 and Arp 74), two systems containing highly disrupted members (WBL 366 and RR 24) and a case of merging in progress (Arp 299, one of the nearest luminous infrared objects).

We detected gas motions following the elongated arm/tail of Arp 70b, while in the fainter member of the pair of galaxies, Arp 70a, the gas distribution is off-centred with respect to the stellar isophotes, suggesting an external acquisition. Our kinematic data highlighted non-circular motions in the velocity field of one of the members of Arp 74 (Arp 74a). The two galaxies of the RR 24 system are connected by one tidal tail, through which the kinematically disturbed component RR 24b seems to supply warm gas to RR 24a. In spite of the nearly irregular gas distribution and perturbed morphology, WBL 366a (the star-forming galaxy VV-523) and WBL 366b have nearly regular velocity fields. The velocity field in the Arp 299 system is irregular, and gas flow between the two nuclei is detected.

The present observations, discussed in the light of model predictions and complementary observations from the literature, suggest that all these systems are still probably in an early phase of the encounter. However, the ionized gas distribution and kinematics are strongly influenced by tidal forces. In particular, cross-fuelling mechanisms between galaxies are in action. In Arp 299 the warm and cold gaseous components show similar kinematic properties, although the cold gas seems to maintain a still better organized motion with respect to the warm gas.

Key words: galaxies: general – galaxies: interactions – galaxies: kinematics and dynamics.

1 INTRODUCTION

Understanding the evolution of small-scale structures in low-density environments (LDE) and of the galaxies they host is a crucial issue in modern cosmology. Although loose, poor groups are the defining structures of LDE, binary galaxies occupy an important place because they are the simplest systems where one can investigate the signatures of interaction. Binaries, ≈10 per cent of the non-clustered population, are also interesting because of the potentially accelerated effects of the secular evolution compared with unpaired galaxies in loose groups.

Observational signatures of secular evolution are indeed present among interacting galaxies. Far-infrared (FIR) studies of pairs (Sulentic 1989; Xu & Sulentic 1991; Hernandez-Toledo & Puerari 1999; Hernandez-Toledo, Dultzin-Hacyan & Sulentic 2001) show unambiguous evidence for interaction-induced star formation in the spiral components of the pairs. Further, recent *ISO* and Hα observations of 17 mixed E + S pairs indicate that some of the early-type components are cross-fuelled by their spiral companions (Domingue et al. 2003). In the secular evolution of galaxies, the gas reservoir then acquires a fundamental importance since it regulates star formation episodes and, probably, feeds the activity of active galactic nuclei (AGN).

Schematically, models of galaxy encounters predict that a galaxy–galaxy interaction influences gas behaviour in two ways. First, a perturber exerts its gravitational force directly upon the gas in the form of a tidal force and makes the gas deviate from its original motion. Secondly, a perturber also deforms the distribution of stars

⋆E-mail: rampazzo@pd.astro.it

in the parent galaxy by tidal forces, and the resulting deformation of the gravitational potential may affect the gas motion. The bar, probably created in the stellar disc as a direct consequence of the tidal force exerted by a perturber, has gained ground as one of the mechanisms able to induce gas flows towards the galaxy centre (see e.g. Noguchi 1988; Gerin, Combes & Athanassoula 1990; Salo 1991; Miwa & Noguchi 1998; Berentzen et al. 2004) since the first phases of an encounter.

Mechanisms like cross-fuelling via small accretions may also be in action (see e.g. Salo & Laurikainen 1993) to feed gas to the galaxy centre. Small accretions of matter should mark the history of galaxies, and not only modify their photometric properties. Indeed, the observed kinematic phenomena retain a memory of the accretion processes driving their formation/evolution. Stellar and gas components with a misaligned or even opposite angular momentum with respect to the host galaxy are often found, not only in early-type galaxies but, recently, also in gas-rich morphological types, like spirals (see e.g. Corsini & Bertola 1998; Bertola et al. 1999; Sarzi et al. 2000; Corsini, Pizzella & Bertola 2002). The statistics of the occurrence of these phenomena is still very poor since they are discovered only by measuring detailed gas and stellar kinematics. We lack an overall picture of the effective weight played by secondary events in shaping Hubble types.

Our understanding of the kinematic behaviour of the different gas components during galaxy encounters seems also to have large uncertainties. There is evidence that the cold gas in shell galaxies, widely considered to be merger remnants, can behave differently from a highly dissipative gas under a tidal interaction (Schiminovich et al. 1994, 1995; Charmandaris, Combes & van der Hulst 2000; Balcells et al. 2001). Charmandaris & Combes (2000) suggest that the dynamics of the cold gas can still be understood in the context of the merging scenario under the hypothesis that the cold interstellar medium is located in dense molecular clouds such as those found in the Milky Way. Owing to their relative compactness (more than 10^3 molecule cm^{-3}, at least 10 times more than in large diffuse gas clouds), molecular clouds are not highly dissipative and tend to behave like stars during a galaxy collision.

It is then crucial to enlarge the set of interacting and merging candidate galaxies for which we have measured stellar and gas (warm and cold) velocity fields in order to shed light on their formation/evolution processes. In this context this paper aims to contribute to the study of the warm gas dynamics during galaxy–galaxy encounters. The paper presents the two-dimensional distribution and kinematics of the ionized gas component of the galaxy members of five interacting, gas-rich systems in LDE. The galaxy systems investigated are mostly isolated pairs, with still distinct members. They differ in nature, from M51-like objects to a merger candidate, and cover different collision parameters.

This paper is organized as follows. Relevant bibliographic data about the galaxies studied in this work are summarized in Section 2. Section 3 gives details on the observations and data reduction. Results are presented in Section 4, including a description of the ionized gas distribution, the velocity field and the determination of galaxy rotation curves. Where possible, the ionized gas kinematics is compared with the available stellar kinematics and, for Arp 74a, a mass model is attempted. Results are finally discussed and summarized in Section 5 in the context of model predictions. We adopted $H_0 = 75$ km s^{-1} Mpc^{-1} throughout this paper.

2 THE SAMPLE: MAIN CHARACTERISTICS

In the following paragraphs, we collect from the literature the characteristics of the observed systems relevant for the present study. Table 1 summarizes the basic kinematic data as available from the literature.

RR 24

This pair is also known as VV 827 (Vorontsov-Velyaminov 1977) and AM 0115−444 (Arp & Madore 1987), and belongs to the Reduzzi & Rampazzo (1995) catalogue of isolated pairs in the Southern hemisphere. Reduzzi & Rampazzo (1996) obtained the 2D ($B - V$) map showing that the colours of the two objects are quite similar and consistent with the late-type morphological classification, although each member is strongly contaminated by the light of the companion (see e.g. Agüero, Paolantonio & Günthard 2000). Their photometry suggests that the distorted structure of the arms is probably created/modified by the on-going interaction. Longhetti et al. (1998b) and Agüero et al. (2000) studied the stellar and gas kinematics of both objects using long-slit spectroscopy. They

Table 1. Basic kinematic data.[a]

Object	Other ID	α (2000)	δ (2000)	Morphology	$V_{\rm hel}$ (km s^{-1})	σ_0 (km s^{-1})	Ref.	D (Mpc)
RR 24a	E2440120	01 18 07	−44 28 00		6852 ± 24	71 ± 31	(1,2)	91
RR 24b	E2440121	01 18 08	−44 27 42		6719 ± 55	80 ± 66	(1,2)	
Arp 70a	VV 341b	01 23 27	30 46 20					140
Arp 70b	VV 341a	01 23 28	30 47 04	S?	10 494			
Arp 74a	UGC 1626	02 08 21	41 28 46	SAB(rs)c	5543 ± 11			74
Arp 74b		02 08 22	41 28 06	IrS				
Arp 299a	NGC 3690, Mkr171	11 28 33	58 33 47	IBm pec	3121 ± 3			41
Arp 299b		11 28 31	58 33 41	SBm? pec	3064 ± 12			
WBL 366a	VV 523, NGC 3991	11 57 31	32 20 16		3192 ± 5			42
WBL 366b	Arp 313a, NGC 3994	11 57 37	32 16 39	SA(r)c pec?	3118 ± 27			
WBL 366c	Arp 313b, NGC 3995	11 57 44	32 17 38	SAm pec	3254 ± 5			

Note. [a]The stellar systemic velocities ($V_{\rm hel}$) and central velocity dispersions (σ_0) of the RR 24 pair members are collected from (1) Agüero et al. (2000) and (2) Longhetti et al. (1998b), respectively. The morphology and the systemic velocities ($V_{\rm hel}$) for the remaining objects are derived from NED (http://nedwww.ipac.caltech.edu/).

measured a systemic velocity separation of ≈133 km s^{-1} and showed that the position–velocity diagram of the ionized gas, along the line connecting the galaxy nuclei (Agüero et al. 2000 used PA = 5°, while Longhetti et al. 1998b used PA = 1°), seems consistent with that of the stars. They further suggest that the 'U' shape of the rotation curve could reflect the on-going interaction during an interpenetrating encounter of the two galaxies (Combes et al. 1995). Longhetti et al. (1998a,b, 1999, 2000) and Agüero et al. (2000) also performed a spectrophotometric study showing that the two nuclei have quite different properties. The southern nucleus (RR 24a) is compatible with an Sb galaxy, while the northern one (RR 24b) has the characteristics of an active star-forming region (Agüero et al. 2000). RR 24 is also a bright infrared (IR) emitter ($L_{\rm FIR} = 1.2 \times 10^{11}$ L$_\odot$). Agüero et al. (2000) suggest that RR24 is a merger candidate whose components are still interacting. Fig. 1(a) shows the Digitized Sky Survey (DSS) image of the system.

Arp 70

This pair, also known as VV 341, is considered an M51-type object by Laurikainen, Salo & Aparicio (1998), who performed a multiband photometric study of this object, providing two-dimensional $(B - V)$ and $(R - I)$ colour maps. Although the systemic velocity of the companion Arp 70a is unknown, the two members are considered interacting by the above authors on the grounds of morphological considerations. Arp 70a shows warps indicating that the companion, Arp 70b, may not be orbiting in the plane of the main galactic disc. Neither of the members have blue $(B - V)$ colour in their nuclei, although the small nuclear $(R - I)$ colour excess would suggest recent star formation (Laurikainen et al. 1998). The DSS image of this pair is shown in Fig. 2(a).

Arp 74

Like the previous object, Arp 74 is considered an M51-type object by Laurikainen et al. (1998). Also in this case, no determination of the systemic velocity of the companion has been made. Thus, the two galaxies are considered interacting only on the grounds of morphological considerations. Arp 74a (UGC 1626) has $(B - V) \approx 0.7$ at the centre, while the outskirts and the companion show $(B - V) = 0.9$ –1. Some zones in the arms of Arp A74a have $(B - V)$ colours between 0.4 and 0.7, indicating the existence of star-forming regions (Laurikainen et al. 1998). Fig. 3(a) shows the DSS image of this system.

The Arp 299 system (NGC 3690)

Arp 299 originally referred to the pair Arp 299a and Arp 299b, the eastern and western members of a merging system composed of two late-type galaxies. Actually, the pair is part of a more complex system of galaxies, which also includes IC 694 (designated also as Arp 299c). In Nilson (1973) the pair Arp 299a+b is associated to NGC 3690, i.e. a single galaxy. In the literature, the eastern member of the merging galaxy pair has often been incorrectly designated as IC 694 and the western member as NGC 3690. As pointed out by Heckman et al. (1999), IC 694 is properly the designation of a small E/S0 galaxy located about 1 arcmin (≈12 kpc) to the north-west of the merging galaxy pair.

The Arp 299 system is one of the nearest luminous infrared galaxies (Sanders & Mirabel 1996) with an estimated star formation rate between 20 and 140 M$_\odot$ yr^{-1} in its discrete star-forming regions (Alonso-Herrero et al. 2000). A near-infrared (NIR) map at 2.1 μm (see fig. 1 in Casoli et al. 1999) shows multiple nuclei. Nordgren et al. (1997) studied the H I morphology of the system Arp 299a+b+c, showing that a tail extends several kiloparsecs away from the stellar body in the northern direction. None of the peaks of the H I emission corresponds to a region of star formation. Also the northern H I tail is offset from the stellar tail. H I and CO kinematics suggest a prograde–retrograde or prograde–polar encounter (Hibbard & Yun 1999; Casoli et al. 1999). Windhorst et al. (2002) using the *HST* WFPC2 studied Arp 299 in the mid-ultraviolet (mid-UV; F255W and F300W filters) and in the *I* band (F814W). They found a large number of young super star clusters throughout the system that they consider in a more advanced phase of merging than the Antennae galaxies, which it resembles. Indeed, there are no obvious bulges in the mid-UV, although NIR images reveal a bulge at least in Arp 299b, the easternmost system. There is also a large quantity of dust within the system. Recently Zezas, Ward & Murray (2003) analysed with *Chandra* the X-ray properties of the Arp 299 system, finding that only 40 per cent of its X-ray luminosity comes from 18 discrete sources, one of which in the Arp 299a nucleus could be a heavily absorbed AGN. The remaining X-ray emission (60 per cent) is thus associated with diffuse hot gas within which the galaxy members are embedded. Fig. 4(a) shows the DSS image of the pair Arp 299.

WBL 366

This group (Vorontsov-Velyaminov 1977; White et al. 1999) is composed of three galaxies, NGC 3991, 3994 and 3995, whose morphology is possibly indicative of an on-going interaction. NGC 3991 (VV 523), a quite blue galaxy [$(U - B) = -0.44$; de Vaucouleurs et al. 1991] is considered a clumpy irregular. It has indeed a chain of numerous H II emission regions of high ionization, with an average size of 300 pc (Hecquet et al. 1995). WBL 366a (NGC 3991) has an estimated rotational mass of 3×10^{10} M$_\odot$ (Hecquet et al. 1995) and is undergoing strong star formation, with star-forming regions having a total mass of about 4×10^7 M$_\odot$. On the other hand, WBL 366b (NGC 3994) and WBL 366c (NGC 3995) are the components of the galaxy pair Arp 313 (VV 249). These two spirals in the group have a vigorous star formation rate (Keel et al. 1985). The H I line morphology (Schneider et al. 1986) indicates the disruption of the outer discs, suggesting a strong interaction between the components of this group. Figs 5(a) and 6(a) show the DSS images of WBL 366a and WBL 366b/c, respectively. The first galaxy is about 4 arcmin (≈49 kpc) to the north-west of the pair WBL 366b/c.

In summary, according to the literature the observed systems should map different stages in gas-rich galaxy–galaxy encounters, from disruptive encounters like those going on in WBL 366 to M51-like systems (Arp 70 and Arp 74) to merging objects (RR 24 and Arp 299).

3 OBSERVATIONS AND DATA REDUCTION

The present set of observations were obtained using three different telescopes and different instrumental configurations, which have in common a Fabry–Perot interferometer and an interference filter inside a focal reducer: the instrument CIGALE,[1] equipped with a new GaAs IPCS was used at the ESO 3.60-m telescope; the instrument CIGALE equipped with a magnetically focused IPCS was used at the

[1] CIGALE (for CInématique des GALaxiEs) is a visiting instrument belonging to the Laboratoire d'Astrophysique de Marseille.

Table 2. Journal of Perot–Fabry observations.

	RR 24	Arp 70	Arp 74	Arp 299	WBL 366
Observations					
Telescope	ESO 3.6 m	SAO 6 m	SAO 6 m	OAN 2.1 m	OAN 2.1 m
Date	2000 Sept. 25	1994 Oct. 8	1994 Oct. 2	2001 Mar. 24	2000 Feb. 6
Interference filter					
Central wavelength (Å)	6590	6801	6688	6620	6620
FWHM (Å)	15	12	23	30	30
Transmission (max.)	0.67	0.60	0.72	0.70	0.70
Calibration					
Neon comp. light (λ, Å)	6598.95	6598.95	6598.95	6598.95	6598.95
Fabry–Perot					
Interference order (at 6562.78 Å)	793	501	501	330	330
Free spectral range (at Hα, km s^{-1})	378	599	599	916	916
Finesse at Hα	12	21	21	24	24
Spec. resolution at Hα	9400 (for S/N=3)	10 000	10 000	8000	8000
Sampling					
No. of scanning steps	32	32	32	48	48
Sampling step (Å)	0.26	0.44	0.44	0.42	0.42
(equiv., km s^{-1})	12	19	19	19	19
Pixel size (arcsec)	0.405	0.84	0.84	1.18	0.59
FOV (arcmin)	3.46	3.58	3.58	5.9	5.9
Detector	GaAs IPCS	Magnetic IPCS	Magnetic IPCS	CCD	CCD
Exposure times					
Total exp. (h)	3.6	1.9	1.7	1.6	3.2
Total exp. time/chan. (s)	405	220	200	120	240
Elem. exp./chan. (s)	15	20	20	120	240

SAO 6-m telescopes; and finally the instrument PUMA,[2] equipped with a charge-coupled device (CCD) was used at the OAN 2.1-m telescope. Contrary to the CCD, IPCS have a zero readout noise, a time resolution of 1/50 s, and a very short readout time, which allows the operator to perform short exposures per channel avoiding transparency changes, typically 5 to 15 s per channel. Several cycles can thus be done and sky changes are averaged. The new IPCS camera, based on GaAs tube technology (Gach et al. 2002), has a quantum efficiency five times higher than the old-generation IPCS, like the magnetically focused IPCS.

RR 24 observations were performed with the CIGALE instrument at the *f*/8 Cassegrain focus of the 3.6-m ESO telescope at La Silla (Chile) and the GaAs IPCS camera. The detector array, 1024 × 1024 pixels, was binned to 512 × 512 and has a pixel size on the sky of 0.405 arcsec for a total field of view (FOV) of 3.46 × 3.46 arcmin^2.

Arp 70 and Arp 74 were observed at the 6-m Special Astrophysical Observatory with CIGALE at the *f*/4 prime focus. CIGALE was coupled to a magnetically focused IPCS, giving 512 × 512 pixels of 30 × 30 μm^2 and a pixel size of 0.84 arcsec, for a total FOV = 3.58 × 3.58 arcmin^2.

Arp 299 and WBL 366 groups were observed with the 2.1-m telescope of the Observatorio Astronómico Nacional at San Pedro Mártir, BC, Mexico (OAN). The PUMA instrument (Rosado et al. 1995) used in these observations was attached to the Cassegrain focus of the OAN 2.1-m telescope. In contrast to the other observations, the detector used with PUMA was a thinned Tektronix CCD of 1024 × 1024 pixels format, with a pixel size of 24 μm (equivalent to 0.59 arcsec on the sky). Only the central 600 × 600 CCD pixels were used. The selected format in the PUMA data cubes (600 × 600 × 48) provides a FOV of 5.9 arcmin on the sky. Table 2 details the journal log and summarizes the main characteristics of the observations.

Reduction of the data cubes was performed using the ADHOCW software (Boulesteix 1999). The data reduction procedure was extensively described in Amram et al. (1996). Wavelength calibration was obtained by scanning the narrow Ne 6599 Å line under the same observation conditions. Velocities measured relative to the systemic velocity are very accurate, with an error of a fraction of a channel width (<3 km s^{-1}) over the whole field. In the case of Arp 299 and WBL 366, the standard CCD data reduction was performed by applying bias and flat-field corrections.

The signal measured along the scanning sequence was separated into two parts: (1) an almost constant level produced by the continuum light in a passband given by the interferential filter around Hα (continuum map), and (2) a varying part produced by the Hα line (Hα integrated flux map). The continuum level was assumed to be the average of the three faintest channels, to avoid channel noise effects. The Hα integrated flux map was obtained by integrating the monochromatic profile in each pixel. The velocity sampling ranges between 12 and 19 km s^{-1}. Strong OH night sky lines

[2] PUMA has been developed for the Observatorio Astronomico Nacional at San Pedro Mártir, BC, Mexico (Rosado et al. 1995).

passing through the channels were subtracted by determining the level of emission away from the galaxies (Laval et al. 1987).

In order to improve the signal-to-noise ratio (S/N), spectral Gaussian smoothing was applied to all data cubes. A spectral smoothing of three channels and a rectangular boxcar smoothing of 3 × 3 pixels were applied to RR 24, Arp 299 and WBL 366, while a spectral smoothing of five channels and a spatial smoothing of 5 × 5 pixels were applied to Arp 70 and Arp 74.

4 RESULTS

4.1 Warm gas distribution and velocity field

From Fabry–Perot observations of RR 24, Arp 70, Arp 74, Arp 299 and WBL 366 (containing the pair Arp 313) we derived the monochromatic, continuum and velocity maps, which we describe in detail below.

RR 24

Fig. 1 displays the Hα monochromatic image and the velocity map of this pair. The monochromatic map (b) highlights two distinct objects. The first one, RR 24b, located to the north, has a nucleus from which two arms, marked by several H II emission regions, stick out. In the southern galaxy, RR 24a, the emission regions appear asymmetrically distributed. In particular, most of the Hα emission of this galaxy comes from its north-west side. This latter object has a higher systemic velocity (see Table 3) than RR 24b and the velocity map (c) reveals the presence of a disc with a nearly regular rotation without an obvious signature of perturbations induced by the interaction with the nearby companion. In contrast, RR 24b does not show a rotation pattern typical of a disc galaxy, which it presumably had before the on-going encounter.

Fig. 1(d) presents a set of Hα line profiles averaged over 11 different zones ($\approx$3 × 3 pixels each, corresponding to 1.2 × 1.2 arcsec^2 and 0.5 × 0.5 kpc^2). Zones 5, 6, 7 and 8 basically cross the minor axis of the RR 24a through the centre and show the presence of two distinct Hα velocity components. The higher-velocity component of this profile (to the right), in each of these zones, represents the emission of RR 24a, roughly at the galaxy systemic velocity. The velocity component at lower velocities (to the left) belongs to the extension of the arm of RR 24b at $V \sim 6750$ km s^{-1} that starts from zone 1. Our measurements do not show evidence of a second gas component connecting the two galaxies in the eastern arm. The velocity components are well separated by about 250 km s^{-1} (see zone 5 in which the two components of the line profile are clearly separated), whereas if a bridge were present, some intermediate velocities would be detected. On the other hand, in (e) we show six zones between the two galaxies following the western arm, which show a continuity in the velocity indicating the presence of a bridge of matter, possibly refuelling gas towards the southern galaxy (RR 24a). The excess of gas visible to the north of the nucleus of RR 24a could be the result of this refuelling. Comparing the relative intensity of the profiles in both arms, we found that the eastern arm is roughly twice as bright as the western arm. This effect could be due to a projection effect indicating that the eastern arm is foreground with respect to the western arm.

Arp 70

Fig. 2 shows the monochromatic and velocity maps of this M51-type pair. The brightest H II region is displaced at about 14 arcsec (9.5 kpc) north from the galaxy centre. The global warm gas velocity amplitude of the main galaxy (Arp 70b) is $\approx$300 km s^{-1}. The velocity field shows a moderately disturbed disc rotation. Arms in Hα appear asymmetric as in the broad-band DSS image. The northern arm is longer than the southern one and is reminiscent of a tail of matter probably induced in the disc by the passage of the companion (Arp 70a, VV 341b). Starting from the disc, along this structure, the gas velocity increases and then drops to the galaxy systemic velocity at its northern edge widely separated from the galaxy centre.

The southern companion galaxy, Arp 70a, is also detected. The Hα emission of the overall galaxy is less intense than several of the H II regions visible in the primary galaxy. Furthermore, the Hα emission seems displaced with respect to the centre of the stellar isophotes. The measured velocity amplitude is $\approx$130 km s^{-1} within the inner 8 arcsec (5.4 kpc).

Arp 74

The monochromatic and velocity maps are shown in Fig. 3. The monochromatic map of Arp 74a, the dominant galaxy in the pair, clearly shows a spiral arm structure characterized by bright H II regions, in particular in the northern arm. The velocity map of Arp 74a presents a disc-like rotation with a maximum velocity gradient of about 113 km s^{-1} (for $i = 52^\circ$) along PA = 75° decoupled from the position angle of the continuum in the outer parts of the galaxy, including the spiral arms (which we estimate at $\approx$130°) and of the inner bar (PA = 45°).

The classification of the companion, Arp 74b, is not given in the literature but the DSS image suggests that it is an early-type object. The galaxy shows a strong Hα emission and a small-amplitude velocity field ($\approx$50 km s^{-1}). The intensity of the central emission is roughly three times brighter than that of the closest H II region belonging to Arp 74a and comparable to the bulge of the latter. Furthermore, the major axis of the stellar component, marked by the continuum, is displaced by about 100°, with respect to the ionized gas kinematic major axis, suggesting an external origin of this component.

The Arp 299 system (NGC 3690)

Fig. 4 shows the Hα emission map and the velocity field of this interacting system. The eastern nucleus shows distinct H II regions (bottom right panel). The brightest continuum peak is shifted by $\approx$4.8 arcsec with respect to the bright Hα peak. Both the Hα emission of the western nucleus and the stellar continuum appear elongated and are composed of subnuclei (see discussion below). At the edge of the Hα distribution, there is an extension of the emission in the north-west direction.

The velocity field is very irregular and no disc rotation pattern is recognizable. There are two regions of high velocities (from orange to red in the bottom right panel of Fig. 4). The western region is reminiscent of a gaseous tail. The velocity difference between the gas located in the western area and the gas near the continuum peak is $\approx$100 km s^{-1}.

The bottom left panel in Fig. 4 shows a close-up of the centres of the two galaxy nuclei. A set of Hα velocity profiles, sampled over the two peaks, are shown. The velocity profiles are complex since a second component is visible. The shape of the velocity profiles changes from pixel to pixel. In zones 6, 7 and 9 the profiles are definitely asymmetric and broader than elsewhere in the galaxy. The velocity profile of zone 8 is still very large since two velocity components are probably mixed. The eastern nucleus, mapped by

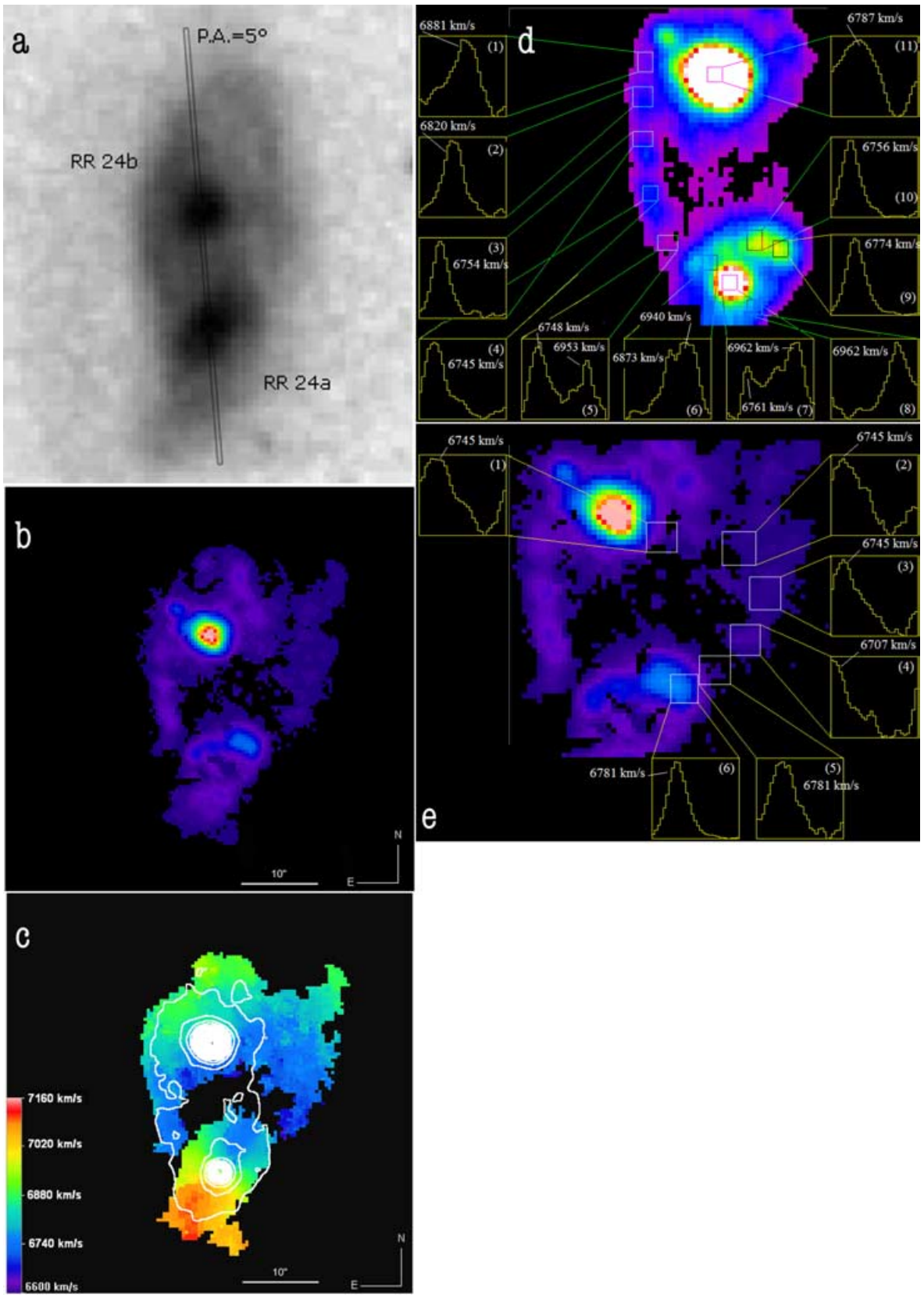

Figure 1. (a) DSS red image of the RR 24 system, showing the slit position angle used by Agüero et al. (2000) to map the gas velocity profile along the line connecting the two galaxy nuclei. (b) Monochromatic Hα image and (c) global velocity field of the warm gas component with the isophotes of the stellar continuum superimposed. (d,e) Warm gas velocity measured in (d) 11 zones along the east arm of RR 24b and (e) six different zones along the west arm/tail; each zone represents a velocity range of 378 km s^{-1} beginning at 6668 km s^{-1}. See text for discussion.

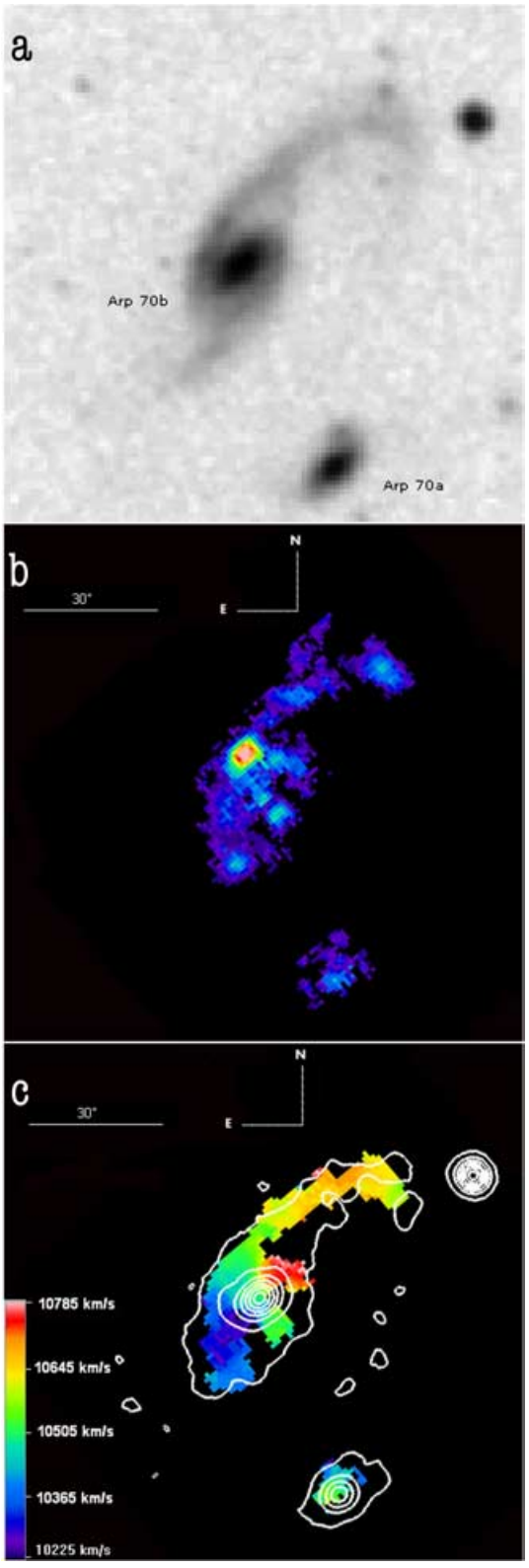

Figure 2. (a) DSS red image of the Arp 70 system. (b) Monochromatic Hα image and (c) velocity field of the warm gas component with the isophotes of the stellar continuum superimposed.

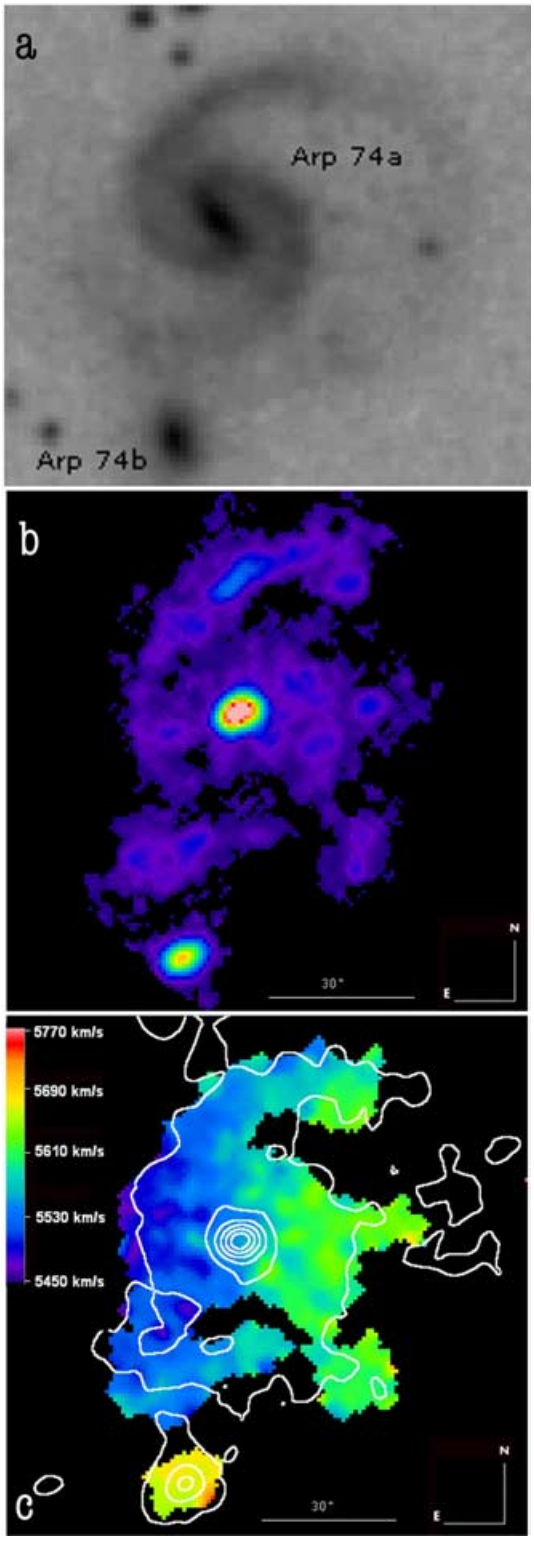

Figure 3. (a) DSS red image of the Arp 74 system. (b) Monochromatic Hα image and (c) velocity field of the warm gas component with the isophotes of the stellar continuum superimposed.

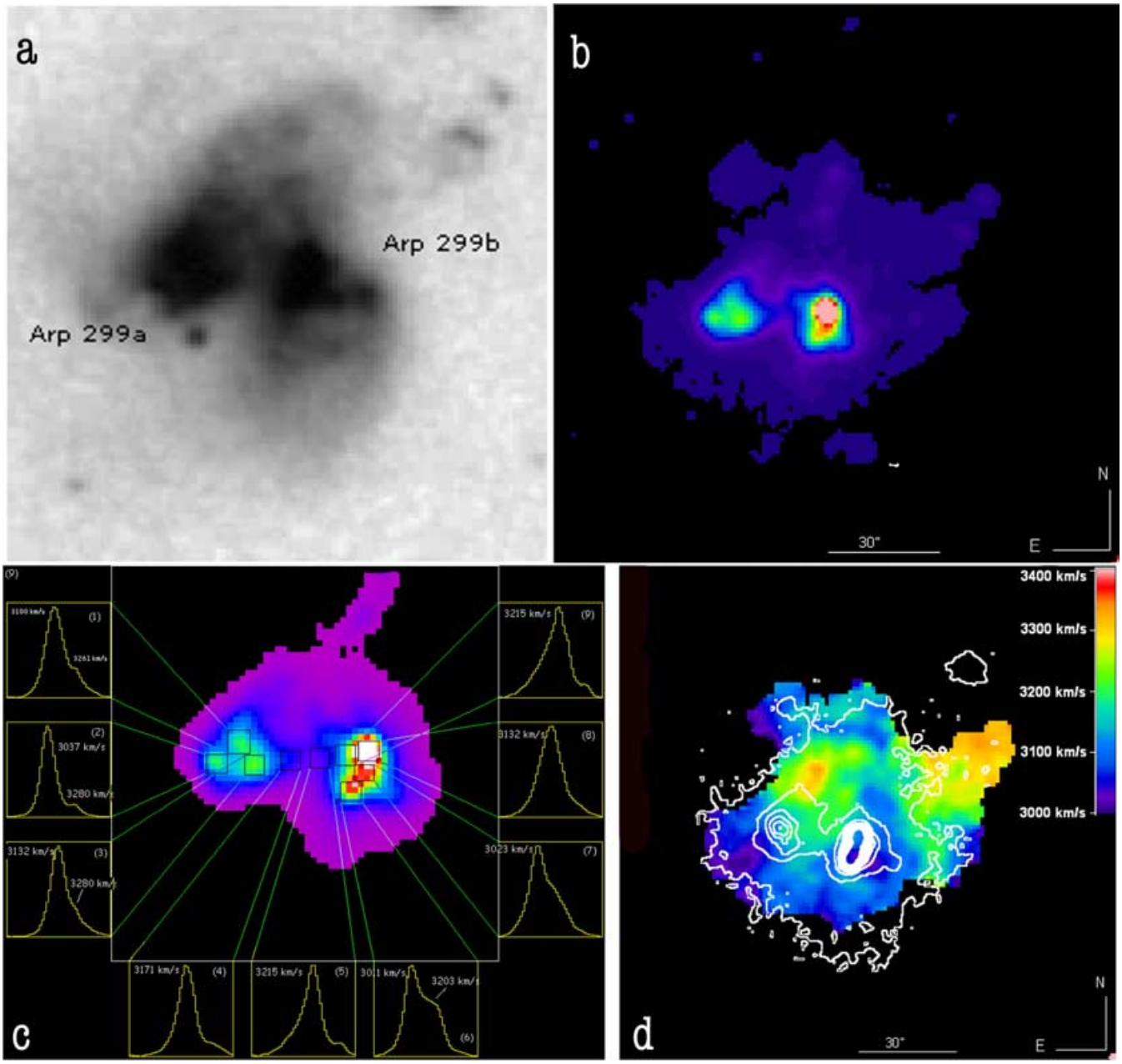

Figure 4. (a) DSS red image of the Arp 299 system (NGC 3690). (b) Monochromatic Hα image. (c) Enlargement of the two galaxy nuclei: velocity measures in nine different zones in the warm gas distribution are shown (see text); each zone represents a velocity range of 916 km s^{-1} beginning at 2673 km s^{-1}. (d) Global velocity field of the warm gas component with the isophotes of the stellar continuum superimposed.

zones 1, 2 and 3, shows a large velocity difference: $\Delta V \approx$ 100 km s^{-1} between the easternmost zone 2 and zone 3. A similar velocity difference is also present between contiguous areas in the western nucleus (areas 8 and 6). Furthermore, areas 3, 4, 5, 8 and 9 show the presence of a connection between the east and west nuclei because of the continuity in the velocity of the component at $V \approx 3200$ km s^{-1}.

WBL 366

In Figs 5 and 6 the Hα and velocity maps of the group members are shown. The monochromatic Hα map of WBL 366a (NGC 3991), quite isolated with respect to the Arp 313 members, has an elongated shape (≈52 arcsec) shown also by the Palomar image. It shows several H II emission knots along the galaxy body, the majority of them being marked in Fig. 5. This galaxy has been classified as a clumpy irregular galaxy by (Hecquet et al. 1995) because of several star formation clumps found. The velocity field, despite the described clumpy distribution of the warm gas, is regular.

Regarding WBL 366b/c (the Arp 313 galaxy pair), the emission regions in NGC 3994 are asymmetrically distributed within the galaxy, and seem to form a gas ring around the galaxy centre. Two small tails point to the north but the bright H II regions are located in the southern part of the galaxy. If we exclude the tails, the velocity field is disc-like, implying a regular rotation. A small emitting region north of the galaxy has been detected. It appears disconnected

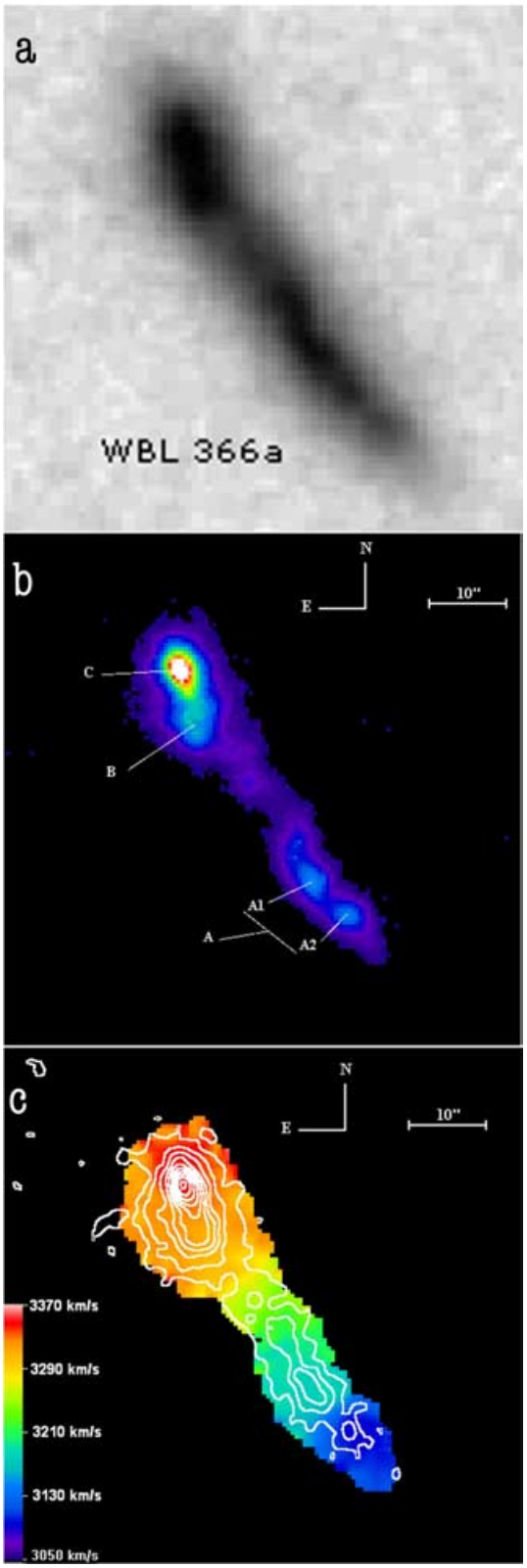

Figure 5. (a) DSS red image of WBL 366a (NGC 3991, VV-523), which together with the Arp 313 pair form the group WBL 366. (b) Monochromatic Hα image and (c) velocity field of the warm gas component with the isophotes of the stellar continuum superimposed. A, B and C are the more intense emission regions in the galaxy (see text).

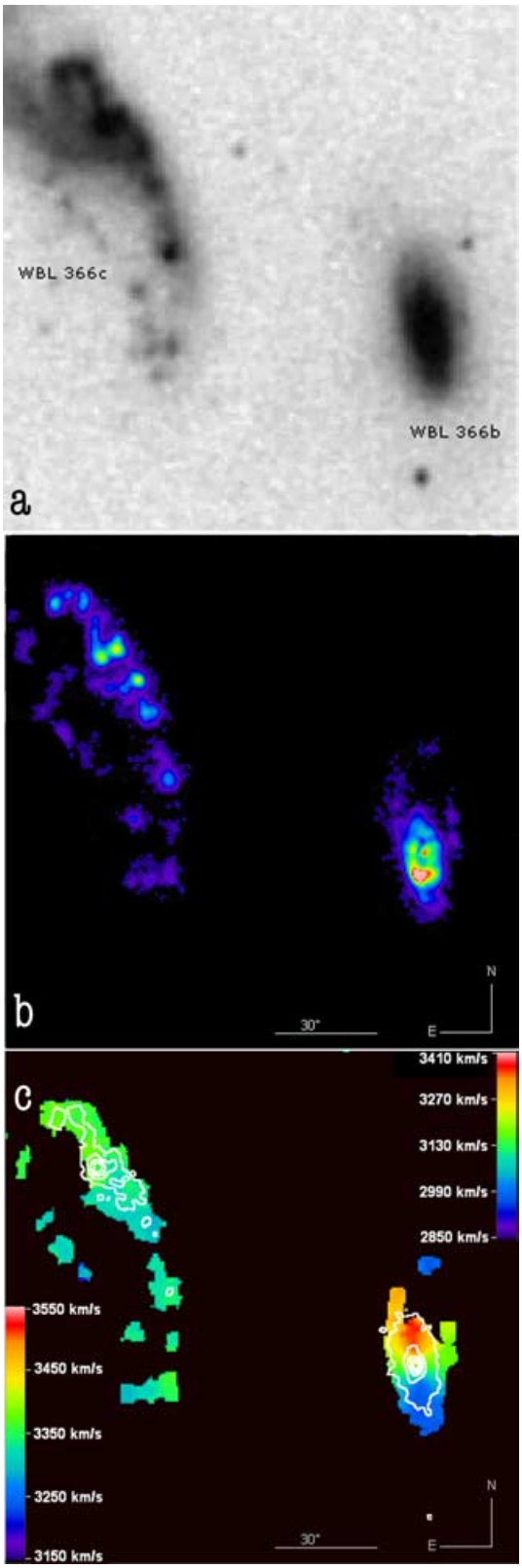

Figure 6. (a) DSS red image of the WBL 366b/c (Arp 313a/b, NGC 3994/3995) system. (b) Monochromatic Hα image of WBL 366b and WBL 366c and (c) velocity field of the warm gas component with the isophotes of the stellar continuum superimposed.

from NGC 3994 with a velocity difference of $\Delta V \approx 330$ km s^{-1} with respect to the northern tail. We did not find a counterpart to this region in the DSS image; however, its continuum level is probably too low to be disentangled from the noise.

In WBL 366c (NGC 3995) the emission regions form an apparent ring-like structure with several knots, also visible in the Palomar image (Fig. 6), but we do not follow the entire structure of the galaxy, in particular the eastern open arm, since it was almost at the edge of the field of view of our PUMA data cubes.

4.2 Rotation curves and velocity profiles

In Fig. 7 we present velocity profiles and rotation curves, along the major axis, for the galaxies in the sample. Because of the velocity incompleteness, we did not derive the rotation curve of WBL 366c. We did not derive the rotation curves of Arp 70b and Arp 299, since they have a very disturbed kinematics.

A Hα long-slit measure of the gas radial velocity distribution was obtained by Agüero et al. (2000) along PA $= 5^\circ$. We simulated a slit aperture, with the same position angle connecting the two galaxy nuclei, in order to derive a velocity curve to be compared with the above long-slit observations (Fig. 7a). In the same panel we also show the stellar velocity profile derived by Longhetti et al. (1998b) along PA $= 1^\circ$. Our Hα velocity profile along this latter position angle is indistinguishable, within the errors, from that shown in the figure. The stellar radial velocity distribution is limited to the very centre of both galaxies. The data of Agüero et al. (2000) agree well with ours for RR 24a but are slightly different (more than the errors quoted in the paper) for RR24b, where their agreement with the stellar component is within error bars. We conclude that the comparison with Longhetti et al. (1998b) shows that the stars and gas rotate in the same sense. While it is difficult to reconstruct the real observing setup of slit observations in the above comparisons, we suggest that velocity zero-point differences between the stellar and gas components, particularly evident for RR 24a, could be explained in the framework of a modest misplacement of the slit with respect to galaxy nuclei.

The rotation curve of RR 24a is given in Fig. 7(b) assuming an inclination of 43° and a PA of 145°, derived from the kinematics. The curve extends up to 11 arcsec (≈5 kpc) and the receding and approaching sides agree very well. There is a plateau at 240 km s^{-1} beginning at ≈4 arcsec (2 kpc). There is no obvious signature of interaction if we exclude the region between 8 and 9.5 arcsec of the approaching side where the western arm possibly influences the curve (the infalling western arm has a lower redshift).

Fig. 7(c) shows the rotation curve of Arp 74a derived by adopting an inclination of 52° and a PA of 75°. The kinematic centre is displaced by about 2.5 arcsec to the north-east with respect to the continuum centre. The rotation curve is peculiar, and both receding and approaching sides match within error bars. The approaching side of the rotation curve has nearly half of the total extension of the receding part. Around 25 arcsec (9 kpc) the rotation curve reaches a plateau at $V = 115$ km s^{-1}.

The velocity profile of the ionized gas component of Arp 74b along PA $= 120^\circ$, i.e. along the major axis set by the isophotes of the continuum, is shown in Fig. 7(d). Fig. 7(e) shows the radial velocity distribution along the line connecting the nuclei of Arp 74a and Arp 74b. Arp 74b shows a velocity gradient on both sides of the galaxy, a sort of 'U' shape, of ≈40 km s^{-1} along PA $= 120^\circ$ and a similar small velocity gradient along PA $= 167^\circ$. Along this latter position angle, i.e. nearly along the galaxy minor axis, the velocity profile appears strongly perturbed. A velocity gradient of ≈60 km s^{-1} is present on the side of the companion but in the opposite direction to the companion's systemic velocity.

We plotted the rotation curve of WBL 366a (Fig. 7f), adopting an inclination of 47° and a PA of 35°. The receding side of the curve is quite flat, reaching a velocity maximum of 133 km s^{-1} at 23 arcsec. This is the position of region C, the brightest star formation area in the galaxy. On the approaching side, the rotation curve has a much more peculiar shape. Beginning at 16 arcsec, the rotation velocity increases from about 100 up to 190 km s^{-1} in less than 5 arcsec and then slowly decreases to 180 km s^{-1}. The H II region marked with A1 corresponds to the beginning of the increasing part of the curve, while the region marked with A2 corresponds to the beginning of the shallow decrease in the rotation curve.

The WBL 366b rotation curve (Fig. 7g) was computed with an inclination of 57° and a position angle of 8°. The kinematic centre is displaced by about 2 arcsec to the north-west with respect to the continuum centre. The approaching side of the curve has a plateau with a velocity of 236 km s^{-1} beginning at 10 arcsec (2 kpc). The receding side is irregular and presents a velocity plateau of 220 km s^{-1} between about 5 and 10 arcsec from the centre, and then decreases to 160 km s^{-1}. The velocity in the plateau between 15 and 25 arcsec corresponds to the north tail velocity.

Either because galaxy surface photometry is not available (as in the case of RR 24a) or because the rotation curve is so disturbed (as in the case of Arp 70b), it was impossible to model the rotation curves using the stellar surface brightness profile except for Arp 74a, for which these data are available.

The method we used in an attempt to model the mass distribution is described in Carignan (1985) and Blais-Ouellette et al. (1999). The stellar luminosity profile is transformed into a mass distribution assuming radially constant mass-to-light ratio. There are therefore three free parameters: the M/L for the luminous matter (disc plus bulge) and two parameters for the dark halo modelled as an isothermal sphere, namely ρ_0, the central density, and r_0, the core radius. A best-fitting routine minimizes the χ^2 in the three-dimensional parameter space.

Fig. 8 shows an attempt to model the rotation curve of Arp 74a using the disc component obtained from the V-band surface brightness profile of Laurikainen & Salo (2001). The best fit of the plateau of the rotation curve, assuming a model of the dark halo with a very low central density and a large core radius, is plotted. At about 20 arcsec from the centre the model reaches a plateau (∼100 km s^{-1} at about 7 kpc). This fitting gives a reasonable $M/L = 2.5$ $M_\odot$ $L_\odot^{-1}$ for the disc (see e.g. Garrido 2003) although no model can properly fit the data, whatever the set of parameters and the dark halo profile used. The result of this fit is not that far from a pure disc model. Even an unrealistic no-disc model could not lead to a much better fit. An NFW (Navarro, Frenk & White 1996) profile, due to its cuspiness, would still degrade the fit as well as the addition of a bulge. Arp 74A is classified in the NED as an SAB(rs)c galaxy, and as an SBc galaxy in the LEDA, which is probably more correct, as it is clear both from its DSS red image (Fig. 3a) and from the surface brightness profile of Laurikainen & Salo (2001) that the bar of this galaxy is strong. The angle between the position angles of the bar (45°) and of the velocity field (75°) is 30°. Following the simulation by Athanassoula (1984), the angular proximity between these two position angles leads to the pronounced signature of the bar in the velocity field and induces the U-shaped rotation curve observed in Arp 74A. We interpreted the residual velocities between the rotation curve derived using the surface photometry and the kinematic rotation curve as the effect of non-circular motions along the bar probably triggered by the interaction.

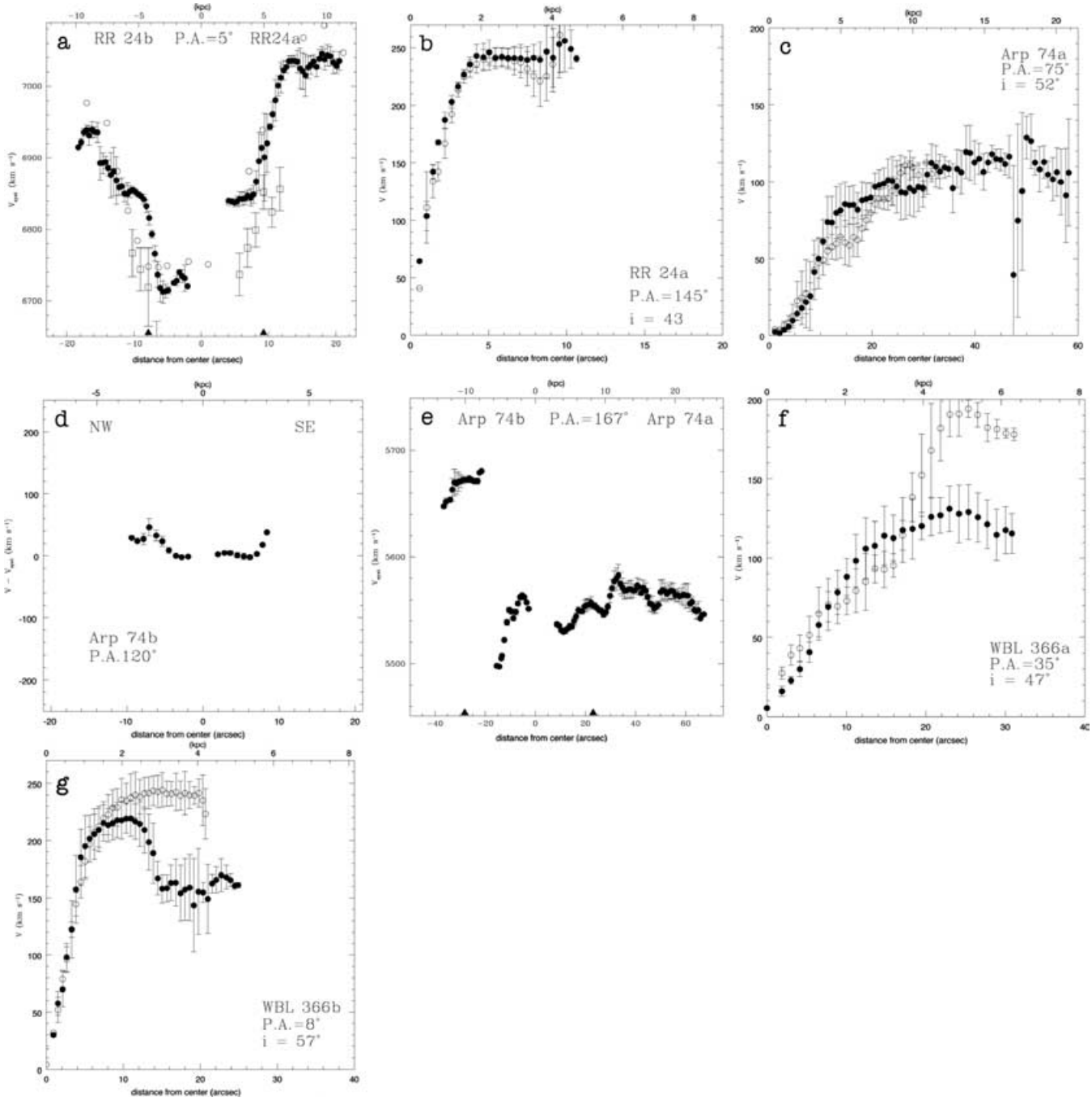

Figure 7. (a) Velocity distribution along the line connecting the nuclei of RR 24a and RR 24b at PA = 5°. Open circles and open squares report the radial velocity distribution of the ionized gas component and the stellar component as measured by Agüero et al. (2000) [the largest measurement errors in the Agüero et al. (2000) data are ≈25 km s^{-1}] and Longhetti et al. (1998b) respectively. (b) Rotation curve of the RR 24a, the southern component of the pair. [In panels (b), (c), (f) and (g) the full and open circles represent the receding and approaching parts of the rotation curve, respectively.] (c) Rotation curve of Arp 74a. (d) Velocity profile along PA = 120° of Arp 74b. (e) Velocity distribution along the line connecting the nuclei of Arp 74a and Arp 74b at PA = 167°. (f) Rotation curve of WBL 366a. (g) Rotation curve of WBL 366c. The distances from the galaxy centre are reported in arcsec (bottom) and kpc (top), adopting distances given in Table 1.

5 DISCUSSION AND CONCLUSIONS

We studied the ionized gas component in five interacting galaxy systems, namely RR 24, Arp 70, Arp 74, Arp 299 and WBL 366, mapping the Hα line. We obtained the warm gas distribution within each member and the gas velocity field. The systemic velocity of galaxies within each pair/group indicates that they form physical systems. Where it was possible to infer the galaxy inclination from the nearly regular kinematics, we determined the rotation curves along the galaxy major axis. In Table 3 we summarize the derived properties of each galaxy, paying attention to the morphology of the warm gas distribution and to the regularity of the velocity field.

Together with the photometric evidence of the secular evolution induced by the interaction, in the Introduction we sketched some

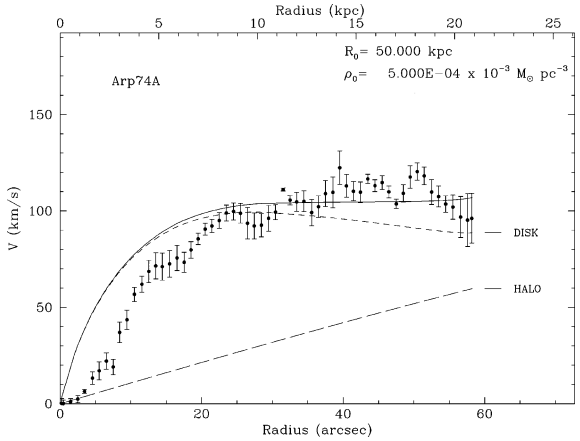

Figure 8. Mass model adopted for the Galaxy Arp 74a (see text). R_0 and ρ_0 are the core radius and the central density of the dark matter, respectively. We assume a spherical and symmetric dark matter distribution following the isothermal sphere profile $\rho(r) = \rho_0/[1 + (r/R_0)^2]$.

kinematic phenomena that are considered signatures of galaxy evolution due to ongoing and/or past interaction episodes. In the light of available simulations we then try to summarize what the warm gas properties could tell us about the evolution of our objects.

Among the basic questions in the study of galaxy–galaxy interaction is the determination of the *phase of encounters*.

M51-type pairs are probably the most simulated kind of objects. Laurikainen et al. (1998) propose that most M51-type pairs represent similar gravitationally bound systems, implying that their star formation properties and spiral patterns are evolving continuously during the course of the orbital evolution. Numerical simulations (see e.g. Laurikainen et al. 1998; Laurikainen & Salo 2001) suggest that M51-type systems, like Arp 70 and Arp 74, could have begun to interact some 10^8 yr ago but the pair may survive for much longer (simulations follow galaxies for 3–4 Gyr). The open arm configuration shown by the simulations of Noguchi (1988) at $T = 2.5$ (i.e 2.5×10^8 yr after the perigalactic passage of the companion; see fig. 1 in his paper) is reminiscent of the Arp 70b morphology, while the presence of a bar, as in Arp 74a, seems to develop later ($\approx 6 \times 10^8$ yr after the perigalactic passage) and it could be maintained in the galaxy stellar component for a much longer period (up to $\approx 25 \times 10^8$ yr). As in the Noguchi (1988) and Salo & Laurikainen (1993) simulations, the warm gas distribution in our data seems to match the gross stellar pattern, although clear departures exist. The large H II region north of the Arp 70b nucleus is not described by models of M51-type pairs (Salo & Laurikainen 1993, 2000), as well as the bar not being visible in the Hα distribution of Arp 74a as is seen in the Noguchi (1988) gas cloud simulations. The effects of the interaction in the gas kinematics are possibly detected in the difference between the kinematic rotation curve and the model of the rotation curve derived from the surface photometry (see Fig. 8). Barton, Bromley & Geller (1999) studied the kinematic effect of tidal interaction on the galaxy rotation curves using an *N*-body code simulating the stellar component. They noticed that the inner disc distorts into a bar-like, elongated structure which has almost no effect on the central part of the rotation curve, the solid-body portion. Our 2D data suggest that in Arp 74a this is not the case when the rotation curve is derived from the warm gas component: non-circular motions can be induced in the gas. The tidal force exerted by the perturber could produce a gas infall towards the nuclear region if the gas dissipates its energy efficiently through cloud–cloud collisions (see also Miwa & Noguchi 1998).

In the simulation of Arp 86, another M51-like system, Salo & Laurikainen (1993) found that a fraction of about 5 per cent of the large galaxy mass can be transferred to the small companion. The off-centring of the warm gas component in Arp 70a with respect to the stellar component suggests that the gas could have been acquired during a fly-by through the main companion disc but it has not yet had time to settle within the galaxy potential.

In the pair RR 24, only one of the interacting objects, RR 24b, shows a quite irregular velocity field and a completely irregular gas distribution. A gas tail joins this galaxy to the companion and possibly it is supplying it with gas. In contrast, RR 24a has a nearly

Table 3. The warm gas component in synthesis.[a]

Object	$V_{\rm hel}$ (km s^{-1})	VF morphology	Warm gas distribution
RR 24a	6940	disc-like	irregular
RR 24b	6749	irregular, west gas tail refuelling RR 24a ?	irregular
Arp 70a	10533		gas displaced from the centre of the stellar continuum
Arp 70b	10492	irregular – tails	largest H II region 14 arcsec N of the centre of the stellar continuum
Arp 74a	5550	irregular	nucleus and spiral arms (1)
Arp 74b	5679		(2)
Arp 299a	3076	irregular, tail	irregular, stellar continuum structures differ from gas structures
	3144		
WBL 366a	3254	regular	elongated, clumpy (2)
WBL 366b	3191	disc-like, tail	clumpy (gas ring ?)
WBL 366c		–	irregular, ring-like (3)

Notes. [a]Column 2 gives the gas systemic velocity measured at the point defined by the centre of the continuum isophotes. In the case of Arp 70a we assumed as systemic the velocity measured in the middle of the field covered by the $H\alpha$ emission which, as shown in Fig. 2, is displaced by a few arcseconds from the centre of the continuum isophotes. Columns 3 and 4 give the morphology of the velocity field and of the warm gas distribution, respectively.
(1) In UGC 1626 the gas has a less regular structure than in the DSS image: the bar is not visible. (2) The gas has a structure very similar to that of the stellar component mapped by the continuum isophotes. (3) The east arm/tail is not within the PUMA field of view (see upper panel in Fig. 5).

regular velocity field. The comparison with the stellar velocity profile (see Fig. 7) shows that stars and gas are coupled, i.e. rotate in the same sense. These properties could suggest that the encounter is still in an early phase since at least one of the members has a disc-like 'kinematic identity'.

Also in the case of the triplet WBL 366 we do not have evidence of an advanced stage of the interaction: only one member, WBL 366c has a really distorted morphology. We lack a complete velocity field of this latter galaxy, but the velocity profile obtained by Keel (1996) (CPG 311b) along PA $= 40^{\circ}$ appears very irregular. The other two members WBL 366b and WBL 366a have a nearly regular, disc-like velocity field, although tails are present and the warm gas distribution is irregular/clumpy, in particular in WBL 366a. We noticed the presence of a detached H II region north of WBL 366b, which has no counterpart in the DSS map. Rubin, Hunter & Ford (1991), describing spiral galaxy kinematics within Hickson compact groups, concluded that their observations support a model in which such groups have only recently accumulated from the lumpy general galaxy distribution: this could also be the origin of WBL 366.

Hibbard & Yun (1999) describe Arp 299 as an on-going merging, with two discs in contact but with still separated nuclei. The above authors calculated that the H I tail has taken at least 7.5×10^8 yr to form, i.e. a time very similar to that taken by objects in M51 pairs, like Arp 74a, to develop their prominent bar as a consequence of the on-going interaction. Our observations show that the warm gas components within the two stellar discs, still easily identifiable in the DSS image, have completely lost their kinematic identity: the velocity field pattern is very irregular. A gas flow between the two nuclei as well as gas tails in the outskirts of the gas distribution are detected. The gas and the stellar kinematics (which we do not have) could then be decoupled. There are several known cases in which stars and warm gas are found to be decoupled, in particular in interacting and/or post-interacting galaxies – like shell galaxies (see e.g. Rampazzo et al. 2003, and reference therein) – and this is well predicted by models (see e.g. Weil & Hernquist 1993).

In the Introduction we mentioned the problem raised by recent shell galaxy observations, i.e. the possibility that the warm and cold gas could behave differently during the evolution of a galaxy–galaxy encounter. A comparison of possible progenitors of shell galaxies, like Arp 299, could be of great value for simulations. The cold gas component in Arp 299 has been traced in detail using CO and H I emissions. Molecular gas in Arp 299 was studied by Casoli et al. (1999). The CO(1–0) map shows three bright regions associated with substructures visible within the nuclei of the galaxies. They indicated, with A, one CO bright region corresponding to our Arp 299a continuum centre (though our Hα region shows three different knots). With B1 and B2, they indicate two bright CO peaks corresponding in Arp 299b to our secondary Hα knots, to the south of our main bright peak, which coincides with the CO peak C. One-third of the entire CO emission comes from this latter star-forming region. While the warm gas component shows an irregular velocity field pattern, the cold gas mapped by the CO(1–0) line (fig. 10 in Casoli et al. 1999) has a nearly regular velocity gradient over the south-eastern part of Arp 299a. In the western part, both the warm and cold gas components have more irregular kinematics. Furthermore, Casoli et al. (1999) noticed that there is a gas flow between Arp 299a and Arp 299b: the above three regions are physically connected as we noticed in our Hα velocity field. *The cold and warm components thus seem to be still partially coupled.* This can also be deduced from the velocity of the components given by Casoli et al. (1999); the A component is at 3110, the B at 3013 and the C at 3154 km s^{-1}, comparable to our velocity values for the kinematic centres of Arp 299a/b determined on the continuum map and reported in Table 3. The disc-like behaviour found in the CO emission in the eastern part of Arp 299a is also confirmed in H I by Hibbard & Yun (1999).

A considerable set of structures visible in the Hα line are detected also in the hot gas phase. This latter in Arp 299 has recently been studied by Zezas et al. (2003) using *Chandra*. In this system 60 per cent of the X-ray emission in the 0.5–8.0 keV band is produced by a diffuse component spatially coincident with regions of widespread star formation. There is a remarkable similarity between the Hα knots and the distribution of discrete X-ray sources in both nuclei of Arp 299, but in particular in Arp 299b. The *Chandra* sources 6 [RA(2000) = 11 28 31.0, $\delta = +58\,33\,41.2$] and 16 [RA(2000) = 11 28 33.7, $\delta = +58\,33\,47.2$] hide two AGN sources that are probably the nuclei of the two interacting galaxies: the positions of these sources correspond to our east (the A nucleus in CO) and south-west nuclei (B1 in CO), marked by the continuum, respectively.

We can thus summarize our results as follows:

(1) The warm gas properties suggest that our sample of interacting systems map different stages of a galaxy–galaxy encounter, but probably with a predominance of early phases in the case of both M51-like systems (Arp 70 and Arp 74) and the apparently more disturbed WBL 366, RR 24, and Arp 299 systems.

(2) Since the beginning of a galaxy–galaxy encounter the gas is strongly influenced by tidal interactions. This gives rise to non-circular motions and gas flows towards the centre of a galaxy and tidal tails that could represent a way to refuel the companion galaxy.

(3) Gas refuelling mechanisms are particularly interesting if the companion is a gas-poor object since it could be a way of inducing secondary star formation episodes.

(4) Interpenetrating encounters, like that of Arp 299, are a very efficient way to mix the gaseous bodies of their progenitors even if the merger episode is not really advanced. In these latter objects, the warm and cold gaseous components show similar kinematic properties, although the cold gas seems to maintain a still better organized motion with respect to the warm gas. The similarity of structures visible in the Hα line and in CO and in the hot gas converge in suggesting an early phase of the encounter.

The determination of 2D velocity maps of the stellar component, lacking for most of the systems, would greatly contribute to the better understanding of the kinematic evolution of these systems. The stellar kinematics could be decoupled from that of the gas not only in Arp 299 but also in M51 companions, like Arp 70a, which could have acquired the gas. In this latter system, which was presumably originally a gas-poor system, a linestrength index analysis would also be of particular interest in order to verify the effect, on the underlying stellar populations, caused by the acquisition of 'fresh' gas.

ACKNOWLEDGMENTS

The work reported herein was based on observations collected at the European Southern Observatory (ESO), La Silla, Chile. We thank the anonymous referee for a very careful reading of the manuscript and for his comments, which helped to improve the presentation and the discussion of the results. We thank Eija Laurikainen for having kindly sent us the luminosity profiles of Arp 70 and Arp 74, and Claude Carignan for allowing us to use his mass model code. MR wishes to acknowledge the financial support from grants IN120802 of DGAPA-UNAM and 2002-C01-40095 of CONACYT. HP wishes

to thank the Laboratoire d'Astrophysique de Marseille (LAM) scientific board for its financial support during a visit in 2004 January–February. This research has made use of the NASA/IPAC Extragalactic Database (NED), which is operated by the Jet Propulsion Laboratory, California Institute of Technology, under contract to the National Aeronautics and Space Administration. The Digitized Sky Survey (DSS) was produced at the Space Telescope Science Institute under US Government grant NAG W-2166. The images of these surveys are based on photographic data obtained using the Oschin Schmidt Telescope on Palomar Mountain and the UK Schmidt Telescope. The plates were processed into the present compressed digital form with the permission of these institutions.

REFERENCES

Agüero E. L., Paolantonio S., Günthard G., 2000, AJ, 122, 94
Alonso-Herrero A., Rieke G. H., Rieke M. J., Scoville N. Z., 2000, ApJ, 532, 845
Amram P., Balkowski C., Boulesteix J., Cayatte V., Marcelin M., Sullivan W., 1996, A&A, 310, 737
Arp H., Madore B. F., 1987, A Catalogue of Southern Peculiar Galaxies and Associations, Cambridge Univ. Press, Cambridge
Athanassoula E., 1984, The Spiral Structure of Galaxies. North-Holland, Amsterdam
Balcells M., van Gorkom J. H., Sancisi R., Del Burgo C., 2001, AJ, 122, 1758
Barton E. J., Bromley B. C., Geller M. J., 1999, ApJ, 511, L25
Berentzen I., Athanassoula E., Heller C. H., Fricke K. J., 2004, MNRAS, 347, 220
Bertola F., Corsini E. M., Vega-Beltrán J., Pizzella A., Sarzi M., Cappellari M., Funes J. G., 1999, ApJ, 519, L127
Blais-Ouelette S., Carignan C., Amram P., Côtè S., 1999, AJ, 118, 2123
Boulesteix J., 1999, User Manual of ADHOCw Reduction Package. Observatoire de Marseille
Carignan C., 1985, ApJ, 299, 59
Casoli F., Willaime M.-C., Viallefond F., Gerin M., 1999, A&A, 346, 663
Charmandaris V., Combes F., 2000, in Valtonen A., Flynn C., eds, ASP. Conf. Ser. Vol. 209, Small Galaxy Groups. Astron. Soc. Pac., San Francisco, p. 273
Charmandaris V., Combes F., van der Hulst J. M., 2000, A&A, 356, L1
Combes F., Rampazzo R., Bonfanti P., Prugniel Ph., Sulentic J. W., 1995, A&A, 297, 37
Corsini E. M., Bertola F., 1998, J. Korean Phys. Soc., 33, 574
Corsini E. M., Pizzella A., Bertola F., 2002, A&A, 382, 48
de Vaucouleurs G., de Vaucouleurs A., Corwin H., Buta R., Paturel G., Fouqué P., 1991, The Third Reference Catalogue of Bright Galaxies. Springer, New York
Domingue D. L., Sulentic J. W., Xu C., Mazzarella J., Gao Y., Rampazzo R., 2003, AJ, 125, 555
Gach J. L. et al., 2002, PASP, 114, 1043
Garrido O., 2003, PhD thesis, Univ. Provence
Gerin M., Combes F., Athanassoula E., 1990, A&A, 230, 37
Heckman T. M., Armus L., Weaver K. A., Wang J., 1999, ApJ, 517, 130
Hecquet J., Augarde R., Coupinot G., Auriere M., 1995, A&A, 298, 726
Hernandez-Toledo H. M., Puerari I., 1999, AJ, 118, 108
Hernandez-Toledo H. M., Dultzin-Hacyan D., Sulentic J. W., 2001, AJ, 121, 1319
Hibbard J. E., Yun M. S., 1999, AJ, 118, 162
Keel W. C., 1996, ApJS, 106, 27
Keel W. C., Kennicutt R. C., Hummel E., van der Hulst J. M., 1985, AJ, 90, 708
Laurikainen E., Salo H., 2001, MNRAS, 324, 685
Laurikainen E., Salo H., Aparicio A., 1998, A&AS, 129, 517
Laval A., Boulesteix J., Georgelin Y. P., Georgelin Y. M., Marcelin M., 1987, A&A, 175, 199
Longhetti M., Rampazzo R., Bressan A., Chiosi C., 1998a, A&AS, 130, 251
Longhetti M., Rampazzo R., Bressan A., Chiosi C., 1998b, A&AS, 130, 267
Longhetti M., Bressan A., Chiosi C., Rampazzo R., 1999, A&A, 345, 419
Longhetti M., Bressan A., Chiosi C., Rampazzo R., 2000, A&A, 353, 917
Miwa T., Noguchi M., 1998, ApJ, 499, 149
Morgan W., 1958, PASP, 70, 364
Mulchaey J. S., Zabludoff A. I., 1999, ApJ, 514, 133
Navarro J. F., Frenk C. S., White S. D. M., 1996, ApJ, 462, 563
Nilson P., 1973, Acta Univ. Upsaliensis, Nova Regiae Societatis Upsaliensis, Ser. V:A, Vol. 1, Uppsala General Catalogue of Galaxies
Noguchi M., 1988, A&A, 203, 259
Nordgren T. E., Chengalur J. N., Salpeter E. E., Terzian Y., 1997, AJ, 114, 77
Rampazzo R., Plana H., Longhetti M., Amram P., Boulesteix J., Gach J.-L., Hernandez O., 2003, MNRAS, 343, 819
Reduzzi L., Rampazzo R., 1995, Astrophys. Lett. Commun., 30, 1
Reduzzi L., Rampazzo R., 1996, A&AS, 116, 515
Rosado M. et al., 1995, RevMexAA Ser. Conf. Vol. 3, The Fifth Mexico–Texas Conf. on Astrophysics, Vol, 3, p. 263
Rubin V. C., Hunter D. A., Ford K. W., 1991, ApJS, 76, 153
Salo H., 1991, A&A, 243, 118
Salo H., Laurikainen E., 1993, ApJ, 410, 586
Salo H., Laurikainen E., 2000, MNRAS, 319, 377
Sanders D. B., Mirabel I. F., 1996, ARA&A, 34, 749
Sarzi M., Corsini E. M., Pizzella A., Vega Beltrán J. C., Cappellari M., Funes J. G., Bertola F., 2000, A&A, 360, 439
Schiminovich D., van Gorkom J. H., van der Hulst J. M., Kasow S., 1994, ApJ, 423, L101
Schiminovich D., van Gorkom J. H., van der Hulst J. M., Malin D. F., 1995, ApJ, 444, L77
Schneider S. E., Helou G., Salpeter E. E., Terzian J., 1986, AJ, 92, 742
Sulentic J. W., 1989, AJ, 98, 2066
Vorontsov-Velyaminov B. A., 1977, A&AS, 28, 1
Weil M., Hernquist L., 1993, ApJ, 405, 142
White R. A., Bliton M., Bhavsar S. P., Bornmann P., Burns J. O., Ledlow M. J., Loken C., 1999, AJ, 118, 2014
Windhorst R. A. et al., 2002, ApJS, 143, 113
Xu C., Sulentic J. W., 1991, ApJ, 374, 407
Zezas A., Ward M. J., Murray S. S., 2003, ApJ, 594, 31

This paper has been typeset from a TEX/LATEX file prepared by the author.